Wannier Diagram and Brown-Zak Fermions of Graphene on Hexagonal Boron-Nitride.

T. Fabian, M. Kausel, L. Linhart, J. Burgdörfer, and F. Libisch*, Institute for Theoretical Physics, TU Wien, 1040 Vienna, Austria, EU *Corresponding author; E-mail: florian.libisch@tuwien.ac.at (Dated: November 3, 2021)

The moiré potential of graphene on hexagonal boron nitride (hBN) generates a supercell sufficiently large as to thread a full magnetic flux quantum Φ_0 for experimentally accessible magnetic field strengths. Close to rational fractions of Φ_0 , $p/q \cdot \Phi_0$, magnetotranslation invariance is restored giving rise to Brown-Zak fermions featuring the same dispersion relation as in the absence of the field. Employing a highly efficient numerical approach we have performed the first realistic simulation of the magnetoconductance for a 250 nm wide graphene ribbon on hexagonal boron nitride using a full ab-initio derived parametrization including strain. The resulting Hofstadter butterfly is analyzed in terms of a novel Wannier diagram for Landau spectra of Dirac particles that includes the lifting of the spin and valley degeneracy by the magnetic field and the moiré potential. This complex diagram can account for many experimentally observed features on a single-particle level, such as spin and valley degeneracy lifting and a non-periodicidy in Φ_0 .

Ultraclean graphene in crystallographic alignment with hexagonal boron nitride (hBN) forms large-scale moiré patterns[1, 2]. The area $S \approx 165 \text{ nm}^2$ of one supercell is large enough to reach the regime of one magnetic flux quantum $\Phi_0 = h/e$ per moiré unit cell already at B = 23.5 T. A plethora of fascinating phenomena emerge such as Hofstadter's butterfly, the fractal energy spectrum of the lattice in the magnetic field [3, 4], Weiss oscillations [5, 6] and Brown-Zak oscillations [7–9], revivals of zero-field conductivity at large magnetic fields periodic in 1/B. Indeed, Hofstadter's butterfly could recently be experimentally observed [10-17]. For exactly rational fractions $p/q \Phi_0$ of the magnetic flux quantum corresponding to magnetic field values $B_{p/q} = p/q \Phi_0/S$, the resulting Bloch wavefunction is strictly periodic and magnetotranslational invariance is restored. Bloch's theorem predicts new quasi-particles, so-called Brown-Zak fermions (BZfs) [7– 9], which travel, undeflected by the magnetic field, ballistically through the moiré superlattice [3, 4, 7–9, 15–24]. Inprints of BZfs in terms of periodic oscillations of the conductance in 1/B (for fixed p), the Brown-Zak oscillations, have been observed up to high temperatures [15, 16].

The large supercell of graphene aligned on hexagonal boron nitride with a linear dimension of $a_S \approx 13.6$ nm includes tenthousands of atoms, rendering numerical simulations of the conductance challenging. Up to now, calculations therefore have focused on the density of states [25–27], a continuum $k \cdot p$ Hamiltonian [24, 28], scaled graphene [29, 30], or on effective 1D models[6]. Here we present, to our knowledge, the first realistic large scale simulation of the conductance for a 250 nm wide graphene on hBN nanoribbon. Our algorithm allows treatment of this multi-scale problem extending from the single atomic scale via the scale of the moiré supercell a_S (= 13 nm) to the width of the nanoribbon W = 250 nm for a wide range of magnetic fields and quasiparticle energies. Even in the absence of any many-body effects we find a remarkably intricate conductance map which reveals many features observed in recent experiments [10–17]. This conductance map can be satisfactorily analyzed by a modified Wannier diagram that features properties of both Dirac-like and Schrödinger-like quasiparticles.

We simulate a ribbon of aligned ($\Theta = 0$) graphene on hexag-

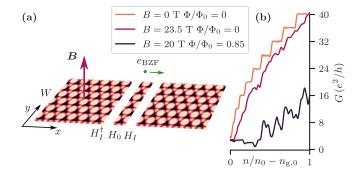


FIG. 1. (a) Build-up of the graphene nanoribbon, schematically. A "slice" of one moiré cell wide described by H_0 is joined by the interaction H_I with adjacent slices to the right and left along the propagation direction of the Brown-Zak Fermion (BZf) x. The width W of the nanoribbon is in y-direction. The magnetic field is oriented perpendicular to the plane of the ribbon. (b) Conductance traces for various magnetic fields as a function of normalized charge carrier density n/n_0 , shifted by the position of the first gap $n_{\rm g,0}$

onal boron nitride in a tight-binding (TB) approximation

$$H = \sum_{i,j} t_{ij} c_i c_j^{\dagger} + \sum_i V_i c_i c_i^{\dagger} + g_s \mu_B \hat{S} \cdot \hat{B}, \qquad (1)$$

with hoppings t_{ij} , on site-potential V_i and a Zeeman term with $g_s = 2$ and Bohr magneton μ_B . The valley degree of freedom of graphene is implicitly contained in the full TB treatment of the lattice and the spin degree of freedom enters through the Zeeman term. We first parametrize the configuration space of the atomistic moiré lattice from a set of ab-initio DFT calculation of primitive cells[31, 32]. We then use a mechanical elasticity model to account for the structural geometry relaxation and induced strain on the graphene layer by the hBN substrate [33, 34] to build an ab-initio derived graphene/hBN structure (see supplement). Unlike most previous theoretical works, we do not use periodic boundary conditions but treat a 250 nm wide ribbon with zig-zag edges locally covered by a Berry-Mondragon potential to suppress edge-states[35]. Since we use a general Bloch ansatz in x-direction, our setup allows us to compute the conductance for arbitrary magnetic fields.

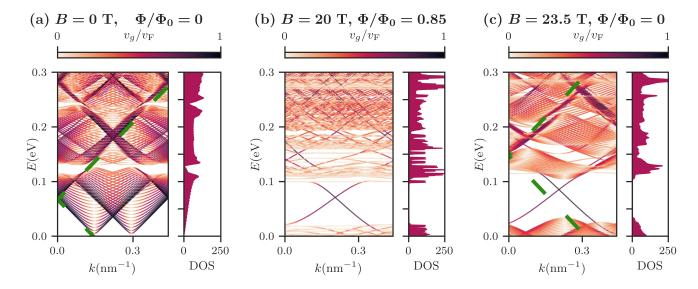


FIG. 2. Band structure and density of states (DOS) in units $n/n_0/eV$ for the magnetic fields (a) B=0 T ($\Phi/\Phi_0=0$), (b) B=20 T ($\Phi/\Phi_0=0.851$), (c) B=23.5 T ($\Phi/\Phi_0=1$). The bandstructure is shaded according to the group velocity relative to v_F , the group velocity of the massless Dirac fermions in (a). The slope $v_g=v_F$ is also indicated in (c) by the green dashed line, where it is shifted according to the minimal coupling $\hbar k - eA$ with A the vector potential.

We compute the bandstructure E(k) of the ribbon for various magnetic fields from

$$\left(H_0 + e^{\mathrm{i}k\Delta x}H_I + e^{-\mathrm{i}k\Delta x}H_I^{\dagger}\right)\psi_n = E_n(k)\psi_n, \qquad (2)$$

where H_0 is the Hamiltonian of a "slice" of the ribbon with a width in *y*-direction of 20 moiré unit cells containing approximately two million sites and H_I the interaction Hamiltonian between adjacent slices (Fig. 1a). The wavevector $k \equiv k_x$ points in propagation direction. To efficiently solve the large but sparse eigenvalue problem of Eq. (2) for eigenvalues $E_n(k)$ and eigenvectors ψ_n close to the Fermi edge, we use the Lanczos method[36, 37] as implemented by the ARPACK library[38].

As our simulation contains the full information on the band structure, the energy axis can be readily transformed into the charge carrier density simply by counting bands. We set n=0 at the charge neutrality point E=0 of graphene and express n in units of $n_0=1/S$, the density of one electron per moiré cell. Likewise, the magnetic field strength B is conveniently expressed in units of magnetic flux quanta through one moiré supercell Φ/Φ_0 .

For each Bloch eigenstate ψ_n the associated group velocity in propagation direction follows from [39]

$$v_g^{(n)} = \frac{1}{\hbar} \frac{\partial E_n(k)}{\partial k} = \frac{i\Delta x}{\hbar} \psi_n^{\dagger} \left(H_I e^{ik\Delta x} - e^{-ik\Delta x} H_I^{\dagger} \right) \psi_n. \quad (3)$$

To efficiently calculate the conductance as function of the energy E, we weight each Bloch state moving in +x-direction of the Brillouin zone, Eq. (2), by the appropriate group velocity, Eq. (3). This weighted density provides an estimate for the conductance G(E) by approximating the number of modes

M(E) at each energy,

$$G(E) = \frac{e^2}{h} M \approx \frac{e^2}{h} \frac{\mathrm{d}}{\mathrm{d}E} \sum_{n: E_n < E} \hbar v_g^{(n)} \, \delta k \tag{4}$$

with a k-point spacing δk . Use of Eq. (4) greatly reduces the computational cost compared to calculation of G(E) using the Landau-Bütticker formalism [40, 41] while yielding nearly identical results (see supplement). Our approach is found to be rather efficient: the characteristic $4e^2/h$ conductance steps of a graphene ribbon at zero field are accurately reproduced [Fig 1 (b)]. This size quantization effect is a consequence of the finite ribbon width W with a subband spacing at B = 0 of the order of 10 meV. The large-scale band structure at zero field (Fig. 2a) features the Dirac cones with linear dispersion emanating from the K and K' points within which the subbands due to transverse size quantization appear. The prominent gap at about $E_{SD} \approx \pi/a_S v_g \approx 120$ meV is caused by the interaction of the primary cones with the backfolded satellite Dirac (SD) cones generated by the moiré potential the strength of which also controls its width $\Delta_m \approx 20$ meV. For a generic strong magnetic field (B = 20 T, or $\Phi/\Phi_0 = 0.851$) chosen not to coincide with a low-order rational $B_{p/q}$, the conductance is dramatically suppressed compared to the field-free case (Fig. 2b), which can be directly traced to the multitude of flat Landau level bands with small group velocities, also visible as pronounced sharp peaks in the density of states (Fig. 2b). However, a further increase of the magnetic field to B = 23.5 T corresponding to $B_{p/q} = B_1$ (or $\Phi = \Phi_0$) leads to an almost complete recovery of the zero-field conductance (Fig. 1c). The associated band structure (Fig. 2c) locally somewhat resembles the zero-field band structure. Most notably, a clustering of Landau subbands with linear slopes close to the slope of the original Dirac cone $v_g \approx v_F$ is observed. It signals the appearance of Brown-Zak

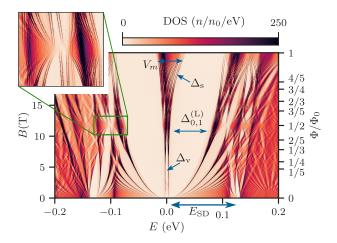


FIG. 3. Density of states (DOS) map as a function of E and B featuring multiple energy scales $E_{SD} \approx \pi/a_S v_g$: spacing between main Dirac cone and moiré induced replica, $\Delta_{n-1,n}^{(L)}$: Landau gaps, Δ_v : broken valley degeneracy, Δ_s : spin splitting, V_m : Broadening near rational Φ/Φ_0 by moiré potential, Inset: zoom into the intersection between Landau level t=-1 and the $\Phi/\Phi_0=1/2$ line, displaying a Hofstadter butterfly.

fermions (BZfs) when magneto-translational invariance is restored for rational fractions of the flux quantum. The width in energy of the segments over which the linear dispersion of BZfs is visible remains, however, limited by the strength of the moiré potential of the order of 20 meV. This perturbative effect of the moiré potential is fundamentally different from BZf spectra in pristine lattices where the zero-field band structure (Fig. 2a) is fully recovered. At large B, the large gap between the lowest Landau level n = 0 and $n = \pm 1$, $\Delta_{0,\pm 1}^{(L)} \approx 100$ meV filled only by two quantum Hall edge states, one for each propagation direction develops Figs. 2(b,c). Smaller gaps remain clearly visible for higher-lying Landau levels (Fig. 2c).

The density of states (DOS) map (Fig. 3) in the E-B plane not only features the prominent Landau gaps easily recognized by the \sqrt{B} dependence of Landau levels of Dirac particles, but also the presence of multiple energy scales in the presence of both the moiré potential and the magnetic field: the gap $E_{\rm SD}\approx 120$ meV due to the moiré-induced secondary Dirac cones, the "broadening" of the Landau levels by $\lesssim 20$ meV at rational Φ/Φ_0 (see, e.g., $\Phi/\Phi_0=1/2$) caused by the formation of the Hofstadter butterfly delimited by the amplitude V_m of the moiré potential, the lifting of the valley degeneracy $\Delta_V\approx 10$ meV by the moiré potential and of the spin degeneracy Δ_S ($\lesssim 3$ meV at $\Phi=\Phi_0$) by the Zeeman term.

The simultaneous presence of multiple energy (and length) scales gives rise to a conductance map of surprising complexity displayed as a function of normalized flux Φ/Φ_0 and normalized carrier density n/n_0 (Fig. 4), featuring several lines of low and high conductance. Lines of high conductance are strictly horizontal at fixed B and are prominent in the projection on the B (or Φ/Φ_0) axis. G(B) is clearly dominated by a sequence of peaks at rational fractions p/q of Φ/Φ_0 and is

periodic in 1/B, the so-called Brown-Zak oscillations [7–9]. Each conductance peak is associated with the ballistic transport of a BZf. The width of each peak is controlled by the effective field $B_{\rm eff}=B-B_{p/q}$. Ballistic transport is suppressed when the effective magnetic length $\lambda_{B_{\rm eff}}=\sqrt{\hbar/(eB_{\rm eff})}$ becomes smaller than the ribbon width $\lambda_{B_{\rm eff}}\ll W$. Accordingly, the peaks of the Brown-Zak oscillations become sharper with increasing ribbon width consistent with recent experimental data for a $17\mu{\rm m}$ wide sample [17].

The conductance maps also features a multitude of intersecting straight lines of conductance minima, or "gaps", with different slopes, widths, and intersections with the n/n_0 axis. A subset of these gaps extend over the entire range of $0 \le \Phi/\Phi_0 \le 1$, while other, less prominent gaps only open for small field regions (see the zoom-in Fig. 4 b). The different types of gaps are well described by using both a modified Wannier diagram for the Landau gaps, taking the linear dispersion of graphene into account, and the usual, "Schrödinger-like" Wannier diagram for lifted degeneracies on a smaller energy scale.

For a system with Schrödinger-like quadratic dispersion originally considered by Hofstadter [3] and Wannier [3] the Landau level energies evolve as function of B according to $E_t^{(S)}(B) = \hbar \omega_B(t+1/2)$ with $t \in \mathbb{N}$ and $\omega_B = eB/m$ the cyclotron frequency. Consequently, the gaps between Landau levels t-1 and t are centered at $E_{g,t}^{(S)} = \hbar \omega_B t$. The normalized charge carrier density up to the Landau gap t follows in form of a Diophantine equation as

$$\frac{n}{n_0} = \int_0^{E_{g,t}^{(S)}} \rho^{(S)}(E) \, \mathrm{d}E + gs = g \left(t \frac{\Phi}{\Phi_0} + s \right)$$
 (5)

with s the number of filled bands at $E_0=0$, g the degeneracy and $\rho(E)=g/(2\pi)$ the constant density of states for fermions with quadratic dispersion in two dimensions. By contrast, the linear dispersion of massless Dirac (D) fermions results in the Landau levels at $E_t^{(D)}(B)=\mathrm{sgn}(t)v_F\sqrt{2\hbar\,|teB|}$ with $t\in\mathbb{Z}$. Here, t=0 corresponds to the zero-energy Landau level, a peculiarity of Dirac fermions [42, 43]. Taking into account the linear increase of the density of states $\rho^{(D)}\propto |E|$, near the Dirac point an analogous calculation immediately yields a modified Diophantine equation for Landau level gaps of graphene near the charge neutrality point

$$\frac{n}{n_0} = g^{(D)}\left(\left(t + \frac{1}{2}\right) \cdot \frac{\Phi}{\Phi_0} + s\right), \qquad s, t \in \mathbb{Z}. \tag{6}$$

with $g^{(D)}$ the degeneracy of the levels on the Dirac cones. For full valley and spin degeneracy $g^{(D)} = 4$. For massless Dirac fermions the minimal degeneracy is $g^{(D)} \ge 2$ due to Fermion doubling, realized as valley degeneracy in graphene, as consequence of the Nielsen–Ninomiya theorem[44]. Thus, the gaps described by Eq. (6) are, despite the half-integer slopes (t+1/2), always a proper subset of those resulting from Eq. (5).

The present results are fully consistent with those for the Hall conductivity. More generaly, the slopes t of the gaps in magnetic field can be expressed by the Hall conductivity $\sigma_{xy} = e\partial n/\partial B|_{E=E_F} = t \cdot e^2/h$. [21, 45]. For graphene, however, a

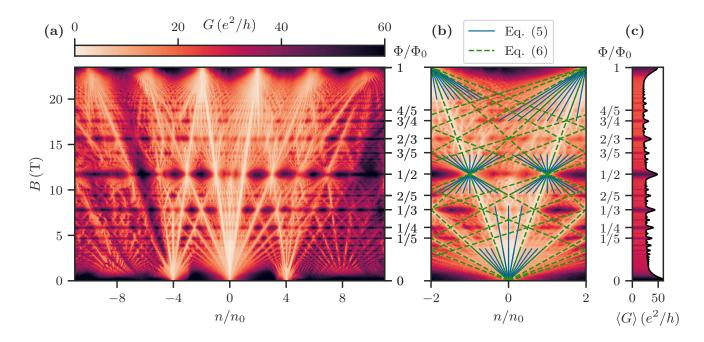


FIG. 4. (a) Conductance map $G(n/n_0, B)$ of a 250 nm wide graphene nanoribbon on hBN. Additional vertical axis Φ/Φ_0 denotes the normalized flux per moiré unit cell. (b) Zoom in of (a), solid blue lines parametrized by the Schrödiner-like Diophantine equation Eq. (5); dashed green lines according to the Dirac Diophantine equation Eq. (6) for Landau gaps. (c) Conductance from (a) averaged over the carrier axis.

characteristic "half integer" Quantum Hall conductance [42, 43] $\sigma_{xy} = g(t+1/2) e^2/h$, $t \in \mathbb{Z}$ has been observed.

If valley and spin degeneracy are strongly broken, the gap structure locally reverts to that predicted by the conventional Diophantine equation (Eq. 5) with g = 1. These additional line segments typically terminate near horizontal lines of BZfs at rational Φ/Φ_0 . This is because the energy scale V_m of the moiré potential forming the BZfs (Fig. 2c) is large compared to the valley degeneracy lifting ΔV (and spin splittings ΔS) generating these gaps. Indeed, the moiré potential is responsible for both inducing a valley degeneracy breaking (ΔV) as well as closing the gaps near rational Φ/Φ_0 by strongly perturbing the Landau levels (Fig. 3). The Wannier formula Eq. (5) is thus only applicable for small intervals of the magnetic field while the Dirac-like Landau gaps Eq. (6) remain visible over the full magnetic field range. Such a complex pattern in the Wannier diagram has been, indeed, observed in recent experiments [10–17]. We emphasize that such complexity emerges from a realistic simulation of graphene on hBN within a single-particle description on the DFT level without invoking any many-body effects. The energy scale for the latter, Δ_{MB} , can be estimated from the flat bands in "magic angle twisted bilayer graphene" [46, 47] and from measurements on bilayer graphene quantum dots[48] to be $\Delta_{MB} \lesssim 1$ meV and, thus, smaller than the energy scales shaping the structures in the Wannier diagram (Fig. 4) in the present case.

One further important structural insight emerging from the Diophantine equation for Dirac fermions (Eq. 6) is that the Wannier diagram is, unlike Eq. (5), and the one for the pristine honeycomb lattice [4], not periodic in Φ_0 . The lines emerg-

ing from $n/n_0 = 0, \pm 4$ at $\Phi = 0$ reach $n/n_0 = \pm 2, \pm 6$ at $\Phi = \Phi_0$. Conversely, lines that would reach $n/n_0 = 0, \pm 4$ at $\Phi = \Phi_0$ are missing. Several experimental data sets [10–17] display, indeed, such an asymmetry which has, to the best of our knowledge, not yet been discussed or explained.

In conclusion, our simulations show in detail the emergence of Brown-Zak fermions in moiré superlattices. We have calculated the magnetoconductance for ab-initio derived, relaxed graphene on hexagonal boron nitride, displaying an intricate fractal pattern caused by Dirac fermions and their satellite cone structures. This pattern is described by a Diophantine equation for Landau gaps of massless Dirac particles. Our single-particle simulation includes lifting of valley and spin degeneracy resulting in a fine structure that locally follows the Diophantine equation for Schrödinger-like particles. The resulting complex Wannier diagram found in agreement with available experimental data can serve as base line to identify possible additional many-body effects not yet included within the single-particle description. We have also clearly demonstrated that the Wannier diagram for Dirac-like particles is non periodic in Φ_0 . Such assymetries have been seen in recent experiments but not yet discussed and analyzed.

I. ACKNOWLEDGEMENTS

We thank C. Stampfer for helpful discussions. The computational results presented have been achieved using the Vienna Scientific Cluster (VSC4).

- [1] C.-H. Park, L. Yang, Y.-W. Son, M. L. Cohen, and S. G. Louie, Phys. Rev. Lett. 101, 126804 (2008).
- [2] M. Yankowitz, J. Xue, D. Cormode, J. D. Sanchez-Yamagishi, K. Watanabe, T. Taniguchi, P. Jarillo-Herrero, P. Jacquod, and B. J. LeRoy, Nature Physics 8, 382 (2012).
- [3] D. R. Hofstadter, Phys. Rev. B 14, 2239 (1976).
- [4] R. Rammal, Journal de Physique **46**, 1345 (1985).
- [5] A. Matulis and F. M. Peeters, Phys. Rev. B **75**, 125429 (2007).
- [6] R. Huber, M.-N. Steffen, M. Drienovsky, A. Sandner, K. Watanabe, T. Taniguchi, D. Pfannkuche, D. Weiss, and J. Eroms, "Brown-zak and weiss oscillations in a gate-tunable graphene superlattice: A unified picture of miniband conductivity," (2021), arXiv:2106.11328.
- [7] E. Brown, Phys. Rev. 133, A1038 (1964).
- [8] J. Zak, Phys. Rev. 134, A1602 (1964).
- [9] J. Zak, Phys. Rev. 134, A1607 (1964).
- [10] L. A. Ponomarenko, R. V. Gorbachev, G. L. Yu, D. C. Elias, R. Jalil, A. A. Patel, A. Mishchenko, A. S. Mayorov, C. R. Woods, J. R. Wallbank, M. Mucha-Kruczynski, B. A. Piot, M. Potemski, I. V. Grigorieva, K. S. Novoselov, F. Guinea, V. I. Fal'ko, and A. K. Geim, Nature 497, 594 (2013).
- [11] C. R. Dean, L. Wang, P. Maher, C. Forsythe, F. Ghahari, Y. Gao, J. Katoch, M. Ishigami, P. Moon, M. Koshino, T. Taniguchi, K. Watanabe, K. L. Shepard, J. Hone, and P. Kim, Nature 497, 598 (2013).
- [12] B. Hunt, J. D. Sanchez-Yamagishi, A. F. Young, M. Yankowitz, B. J. LeRoy, K. Watanabe, T. Taniguchi, P. Moon, M. Koshino, P. Jarillo-Herrero, and R. C. Ashoori, Science 340, 1427 (2013), https://science.sciencemag.org/content/340/6139/1427.full.pdf.
- [13] G. L. Yu, R. V. Gorbachev, J. S. Tu, A. V. Kretinin, Y. Cao, R. Jalil, F. Withers, L. A. Ponomarenko, B. A. Piot, M. Potemski, D. C. Elias, X. Chen, K. Watanabe, T. Taniguchi, I. V. Grigorieva, K. S. Novoselov, V. I. Fal'ko, A. K. Geim, and A. Mishchenko, Nature Physics 10, 525 (2014).
- [14] L. Wang, Y. Gao, B. Wen, Z. Han, T. Taniguchi, Watanabe, J. M. Koshino, Hone, K. and R. Dean. Science **350**. 1231 C., (2015).https://science.sciencemag.org/content/350/6265/1231.full.pdf.
- [15] R. Krishna Kumar, X. Chen, G. H. Auton, A. Mishchenko, D. A. Bandurin, S. V. Morozov, Y. Cao, E. Khestanova, M. Ben Shalom, A. V. Kretinin, K. S. Novoselov, L. Eaves, I. V. Grigorieva, L. A. Ponomarenko, V. I. Fal'ko, and A. K. Geim, Science 357, 181 (2017), https://science.sciencemag.org/content/357/6347/181.full.pdf.
- [16] R. Krishna Kumar, A. Mishchenko, X. Chen, S. Pezzini, G. H. Auton, L. A. Ponomarenko, U. Zeitler, L. Eaves, V. I. Fal'ko, and A. K. Geim, Proceedings of the National Academy of Sciences 115, 5135 (2018), https://www.pnas.org/content/115/20/5135.full.pdf.
- [17] J. Barrier, P. Kumaravadivel, R. Krishna Kumar, L. A. Ponomarenko, N. Xin, M. Holwill, C. Mullan, M. Kim, R. V. Gorbachev, M. D. Thompson, J. R. Prance, T. Taniguchi, K. Watanabe, I. V. Grigorieva, K. S. Novoselov, A. Mishchenko, V. I. Fal'ko, A. K. Geim, and A. I. Berdyugin, Nature Communications 11, 5756 (2020).
- [18] F. Bloch, Zeitschrift für Physik **52**, 555 (1929).
- [19] M. Y. Azbel, Sov. Phys. JETP 19, 634 (1964).
- [20] G. H. Wannier, physica status solidi (b) 88, 757 (1978), https://onlinelibrary.wiley.com/doi/pdf/10.1002/pssb.2220880243.
- [21] P. Streda, Journal of Physics C: Solid State Physics 15, L717 (1982).

- [22] J.-W. Rhim and K. Park, Physical Review B 86, 235411 (2012).
- [23] P. Delplace and G. Montambaux, Physical Review B 82, 035438 (2010).
- [24] X. Chen, J. R. Wallbank, A. A. Patel, M. Mucha-Kruczyński, E. McCann, and V. I. Fal'ko, Phys. Rev. B 89, 075401 (2014).
- [25] L. A. Chizhova, F. Libisch, and J. Burgdörfer, Phys. Rev. B 90, 165404 (2014).
- [26] J. Jung, A. Raoux, Z. Qiao, and A. H. MacDonald, Phys. Rev. B 89, 205414 (2014).
- [27] J. Jung, A. M. DaSilva, A. H. MacDonald, and S. Adam, Nature Communications 6, 6308 (2015).
- [28] G. Chen, M. Sui, D. Wang, S. Wang, J. Jung, P. Moon, S. Adam, K. Watanabe, T. Taniguchi, S. Zhou, M. Koshino, G. Zhang, and Y. Zhang, Nano Letters 17, 3576 (2017).
- [29] M.-H. Liu, P. Rickhaus, P. Makk, E. Tóvári, R. Maurand, F. Tkatschenko, M. Weiss, C. Schönenberger, and K. Richter, Phys. Rev. Lett. 114, 036601 (2015).
- [30] S.-C. Chen, R. Kraft, R. Danneau, K. Richter, and M.-H. Liu, Communications Physics 3, 71 (2020).
- [31] R. Bistritzer and A. H. MacDonald, Phys. Rev. B 84, 035440 (2011).
- [32] J. Quan, L. Linhart, M.-L. Lin, D. Lee, J. Zhu, C.-Y. Wang, W.-T. Hsu, J. Choi, J. Embley, C. Young, T. Taniguchi, K. Watanabe, C.-K. Shih, K. Lai, A. H. MacDonald, P.-H. Tan, F. Libisch, and X. Li, Nature Materials 20, 1100 (2021).
- [33] N. N. T. Nam and M. Koshino, Physical Review B 96 (2017), 10.1103/physrevb.96.075311.
- [34] S. Carr, D. Massatt, S. B. Torrisi, P. Cazeaux, M. Luskin, and E. Kaxiras, Physical Review B 98 (2018), 10.1103/physrevb.98.224102.
- [35] M. V. Berry and R. J. Mondragon, Proceedings of the Royal Society of London. A. Mathematical and Physical Sciences 412, 53 (1987), https://royalsocietypublishing.org/doi/pdf/10.1098/rspa.1987.0080.
- [36] C. Lanczos (1950).
- [37] G. H. Golub and H. A. van der Vorst, Journal of Computational and Applied Mathematics 123, 35 (2000), numerical Analysis 2000. Vol. III: Linear Algebra.
- [38] R. Lehoucq, D. Sorensen, and C. Yang, "Arpack users' guide: Solution of large scale eigenvalue problems with implicitly restarted Arnoldi methods," (1997).
- [39] I. Rungger and S. Sanvito, Phys. Rev. B 78, 035407 (2008).
- [40] R. Landauer, IBM Journal of Research and Development 1, 223 (1957)
- [41] M. Büttiker, Phys. Rev. B 38, 9375 (1988).
- [42] Y. Zhang, Y.-W. Tan, H. L. Stormer, and P. Kim, Nature 438, 201 (2005).
- [43] K. S. Novoselov, A. K. Geim, S. V. Morozov, D. Jiang, M. I. Katsnelson, I. V. Grigorieva, S. V. Dubonos, and A. A. Firsov, Nature 438, 197 (2005).
- [44] H. Nielsen and M. Ninomiya, Nuclear Physics B **185**, 20 (1981).
- [45] D. J. Thouless, M. Kohmoto, M. P. Nightingale, and M. den Nijs, Phys. Rev. Lett. 49, 405 (1982).
- [46] Y. Cao, V. Fatemi, S. Fang, K. Watanabe, T. Taniguchi, E. Kaxiras, and P. Jarillo-Herrero, Nature **556**, 43 (2018).
- [47] M. Yankowitz, S. Chen, H. Polshyn, Y. Zhang, K. Watanabe, T. Taniguchi, D. Graf, A. F. Young, and C. R. Dean, Science 363, 1059 (2019), https://science.sciencemag.org/content/363/6431/1059.full.pdf.
- [48] S. Möller, L. Banszerus, A. Knothe, C. Steiner, E. Icking, S. Trellenkamp, F. Lentz, K. Watanabe, T. Taniguchi, L. Glaz-

man, V. Fal'ko, C. Volk, and C. Stampfer, "Probing two-

electron multiplets in bilayer graphene quantum dots," (2021), arXiv:2106.08405.